Journal of Solid State Chemistry 183 (2010) 186–191

Contents lists available at ScienceDirect

Journal of Solid State Chemistry

journal homepage: www.elsevier.com/locate/jssc

Crystal structure of the monoclinic and cubic polymorphs of $BiMn_7O_{12}$

H. Okamoto [a], N. Imamura [b], M. Karppinen [b,c], H. Yamauchi [b,c], H. Fjellvåg [a,*]

[a] Centre for Materials Science and Nanotechnology, Department of Chemistry, University of Oslo, P.O. Box 1033 Blindern, NO-0315 Oslo, Norway
[b] Materials and Structures Laboratory, Tokyo Institute of Technology, Yokohama 226-8503, Japan
[c] Laboratory of Inorganic Chemistry, Department of Chemistry, Helsinki University of Technology, FI-02015 TKK, Finland

ARTICLE INFO

Article history:
Received 5 August 2009
Received in revised form
20 October 2009
Accepted 22 October 2009
Available online 28 October 2009

Keywords:
Perovskite
Manganese
Crystal structure
Synchrotron X-ray diffraction

ABSTRACT

The complex perovskite $BiMn_7O_{12}$ occurs with two polymorphic structures, cubic and monoclinic. Currently their crystal structures are investigated with high-resolution synchrotron powder X-ray diffraction at room temperature. Rietveld analysis reveals unusual behavior for, respectively, the oxygen and bismuth atoms in the monoclinic and cubic phases. Bond valence calculations indicate that all the Mn atoms in both the phases are in trivalent state. Possible roles of the $6s^2$ lone-pair electrons of Bi^{3+} in $BiMn_7O_{12}$ are discussed in comparison with the $LaMn_7O_{12}$ phase that is isomorphic to monoclinic $BiMn_7O_{12}$. Multiple roles of the lone-pair electrons are revealed, causing (i) *A*-site cation deficiency, (ii) octahedral tilting, (iii) *A*-site cation displacement, and (iv) Mn^{3+} Jahn–Teller (JT) distortion. Relationships between the monoclinic and cubic phases are discussed with emphasis on the MnO_2 and MnO_6 local structural aspects. All Mn atoms in the monoclinic polymorph have distorted coordination consistent with JT-active Mn(III) high spin, whereas for the cubic polymorph, the *B*-site Mn atoms show regular octahedral coordination.

1. Introduction

Complex transition metal oxides have high potential for novel functionalities. Among such oxides, the bismuth manganese perovskite oxide, $BiMnO_3$ has been intensively studied as a multiferroic material [1–6]. The oxide is unique since it exhibits ferromagnetic ordering at low temperatures, i.e. $T_C \approx 105$ K [2–4]. This is striking when compared to $LaMnO_3$ that exhibits antiferromagnetic ordering (of *A*-type [7]) in spite of the fact that the ionic radius of La^{3+} (1.30 Å for 8-coordination [8]) is almost identical to that of Bi^{3+} (1.31 Å for 8-coordination [8]). The uncommon properties of $BiMnO_3$ are likely to appear due to the $6s^2$ lone-pair electrons of Bi^{3+}. The lone-pair induces an additional distortion of the lattice which turns monoclinic (space group *C*2 [6]), and the resultant off-center atomic displacement gives rise to polar characteristics.

The related 1-to-3 (or 1:3) *A*-site ordered perovskite oxide, $A'Mn_7O_{12}$ [$(A'Mn_3)_A(Mn_4)_BO_{12}$] was first reported in the early 1970s for $A'=Na^+$, Ca^{2+}, Cd^{2+}, Sr^{2+}, La^{3+} and Nd^{3+} [9,10]. Not only $A'Mn_7O_{12}$ but the related *A*-site ordered oxides (e.g. $A'Cu_3Mn_4O_{12}$) take a $2\times2\times2$ unit-cell in terms of the simple perovskite structure [see Fig. 1(a)]. Most of such oxides are synthesized under high pressures (~5 GPa) to stabilize a strongly distorted 12-coordination for Mn^{3+} (and Cu^{2+}) at the *A*-site [see Fig. 1(b)]. Depending on the oxidation state of the *A*′-site cation, the crystal structure of $A'Mn_7O_{12}$ varies from cubic (space group $Im\bar{3}$) for $A'=Na^+$, *via* trigonal (space group $R\bar{3}$) for $A'=Ca^{2+}/Cd^{2+}$ to monoclinic (space group *I*2/*m*) for $A'=La^{3+}/Nd^{3+}$ at room temperature [9,10]. It has been suggested that Jahn–Teller (JT) active species, Mn^{3+} or Cu^{2+}, are required at the *A*″-site to stabilize the 1:3 *A*-site ordering, while the oxidation state of Mn at the *B*-site may vary depending on the (average) charge of the *A*-site cation(s).

Among such 1:3 *A*-site ordered compounds, $BiCu_3Mn_4O_{12}$ was reported to exhibit half metallic nature [11]. The material shows ferromagnetic ordering below $T_C=350$ K. The Cu-free analog, $BiMn_7O_{12}$, takes the same monoclinic *I*2/*m* structure as that of $LaMn_7O_{12}$, but exhibits two transitions, ferromagnetic- and antiferromagnetic-like at 59 and 28 K, respectively [12]. While finalizing this manuscript, Mezzadri et al. [13] pointed out that the off-center displacement of Bi in $BiMn_7O_{12}$ results in a subsequent reduction in symmetry *Im* and thus $BiMn_7O_{12}$ would not be isomorphic with $LaMn_7O_{12}$. Their analysis being based on single-crystal X-ray diffraction data supports the possibility of a multiferroic nature of $BiMn_7O_{12}$.

Usually Bi^{3+} and La^{3+} have essentially equal ionic radii, though the size of Bi^{3+} depends on the $6s^2$ lone-pair electron effect. When bismuth is forced into high symmetry structures, the size of Bi^{3+} appears less than that of La^{3+}, while a dominant lone-pair

* Corresponding author. Fax: +47 22 85 54 41.
E-mail addresses: hiroshi.okamoto@kjemi.uio.no (H. Okamoto).
helmer.fjellvag@kjemi.uio.no (H. Fjellvåg).

0022-4596/$ - see front matter © 2009 Elsevier Inc. All rights reserved.
doi:10.1016/j.jssc.2009.10.013

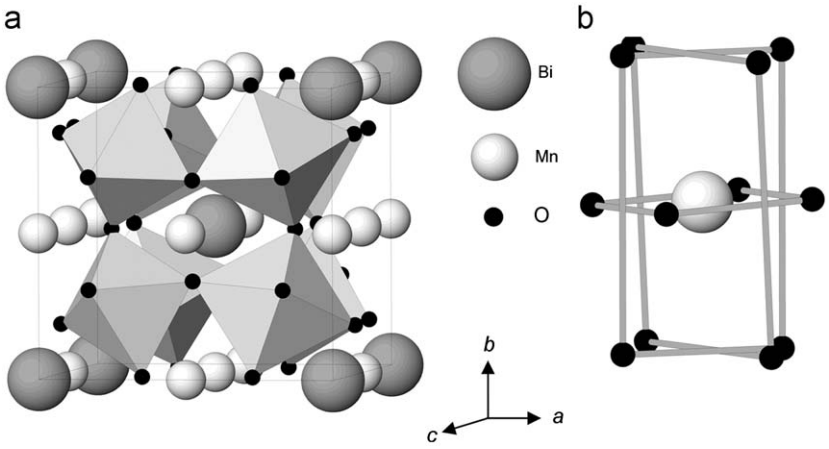

Fig. 1. Schematic drawing of the crystal structure of (a) $BiMn_7O_{12}$ and (b) the strongly distorted MnO_{12} coordination at the *A*-site.

electron character creates structural distortion and a possible volume expansion beyond that observed for a corresponding La^{3+} compound. For example, when $BiTaO_4$ transforms from a structure for which the lone-pair electron character is dominant to the $LaTaO_4$ structure, it undergoes a volume reduction owing to local crystal structure distortions around the Bi-ions [8]. Thus, the size of Bi^{3+} depends on the degree of $6s^2$ lone-pair electron effect.

In the present study, we show that $BiMn_7O_{12}$ exists in two polymorphs, cubic and monoclinic (but notably not trigonal). This is intriguing in light of the large difference in chemical properties of the *A*′-site cation in the cubic and monoclinic variants of $A'Mn_7O_{12}$ with $A'=Na^+$ and La^{3+}, respectively. A key to understanding this is probably the $6s^2$ lone-pair electron character for Bi^{3+}, *cf.* its role in introducing rather unique properties in $BiMnO_3$. Here we address two important issues: (i) the trigger for the formation of cubic and monoclinic polymorphs in $BiMn_7O_{12}$, and (ii) the state of Bi^{3+} cation with respect to lone-pair electrons. The crystal structures of cubic and monoclinic $BiMn_7O_{12}$ are described on the basis of high-resolution synchrotron powder X-ray diffraction data (HRSXRD). We first discuss the structure of monoclinic $BiMn_7O_{12}$ in comparison to that of isostructural $LaMn_7O_{12}$. Thereafter we discuss structural features of cubic $BiMn_7O_{12}$ in comparison with those of the monoclinic polymorph.

2. Experimental

Samples of the monoclinic and cubic $BiMn_7O_{12}$ polymorphs were prepared by high pressure synthesis. Final firing under high pressure of 5 GPa was employed for starting materials of Bi_2O_3 and Mn_2O_3 for the monoclinic phase. For the cubic polymorph, the intermediate ternary products $Bi_2Mn_4O_{10}$ and $Bi_{12}MnO_{20}$ as well as binary oxides of Bi_2O_3 and Mn_2O_3 after calcination were used as starting reactants (for details, see Ref. [14]). Compositional analysis was performed by ICP-AES (inductively coupled plasma atomic emission spectrometer: Shimadzu ICPS-8100) with a precision of 95% (see details in Ref. [14]). Phase purity of the derived products was investigated by conventional X-ray diffraction using Cu*K*α radiation (Rigaku: RINT2000$^+$ ultraX18). Unit-cell dimensions and atomic coordinates were determined through Rietveld refinements [15] using the GSAS code [16] and based on HRSXRD data collected at room temperature with the high-resolution diffractometer at Swiss–Norwegian Beam Lines (BM01B), European Synchrotron Radiation Facility (ESRF), using radiation with wavelength $\lambda=0.52019$ Å. Crushed fine powders were kept in 0.50 mm rotating borosilicate capillaries, open to the air. The HRSXRD patterns were measured over the scattering range $3.000^\circ \le 2\theta \le 45.000^\circ$ with 0.002°/min sweeping scan mode. One peak from $Bi_2O_2CO_3$ can be identified at low angle in the HRSXRD patterns. Judging from the relative peak intensities, and Rietveld refinements, the impurity content is estimated as ~0.02 wt% maximum. It is worth noting that this is likely to apply also for the samples earlier investigated by ICP. One scale factor, zero point, five pseudo-Voigt profile parameters, four (monoclinic phase) and/or one (cubic phase) unit-cell dimensions entered into the final least-squares refinements. Details of the positional parameters and isotropic displacement factors in the Rietveld refinements are given below.

3. Results and discussion

Monoclinic phase: The HRSXRD pattern for the monoclinic phase is shown in Fig. 2(a). Indexing of the diffraction data confirmed a single phase sample with a monoclinic unit-cell and lattice parameters, $a=7.5191(1)$ Å, $b=7.3652(1)$ Å, $c=7.5284(1)$ Å, and $\beta=91.225(1)^\circ$. The inset to Fig. 1(a) is in accordance with the systematic reflection conditions: $h\,k\,l$: $h+k+l=2n$ corresponding to a body centred monoclinic cell [see Fig. 2(a)]. Possible space groups are *I*2 (No. 5), *Im* (No. 8), and *I*2/*m* (No. 12). In the present study the highest symmetrical space group, *I*2/*m*, is adopted, though Mezzadri et al. [13] recently reported that space group *Im* is likely to be correct.

During initial refinements, occupancies of the *A*′-site Bi, *A*″-site Mn, and *B*-site Mn converged respectively to 0.97(1), 0.99(1), and 1.00(1). Henceforth, the occupancies of both the *A*″- and *B*-site Mn atoms were fixed to unity, whereas the occupancy of Bi was still varied during the final refinement. The results show that the composition of the monoclinic phase is essentially stoichiometric, i.e. $BiMn_7O_{12}$. The final refinement results for the fully stoichiometric phase are given in Table 1. It is worth noting that the isotropic displacement parameter (U_{iso}) took anomalously large values, i.e. 2.40(4) Å^2, 1.96(3) Å^2, and 4.3(1) Å^2 for *A*″-site Mn, *B*-site Mn, and O, respectively, whereas the refined value was 1.37(2) Å^2 for Bi. The former values are unusually large when compared with those for well ordered perovskite-type materials. Individual U_{iso} refinements for the non-equivalent O atoms yielded the values, 4.3(3) Å^2, 3.7(7) Å^2, 5.9(3) Å^2, and $3.2(2)\times10^{-2}$ Å^2 for O1, O2, O3, and O4 (the latter two taking general *x*,*y*,*z*-sites), respectively.

The average formal oxidation state of all manganese atoms is close to III according to the chemical composition. For the *B*-site octahedral environment such $3d^4$ species are expected to show a JT distortion in the high spin state. The bond distances in the

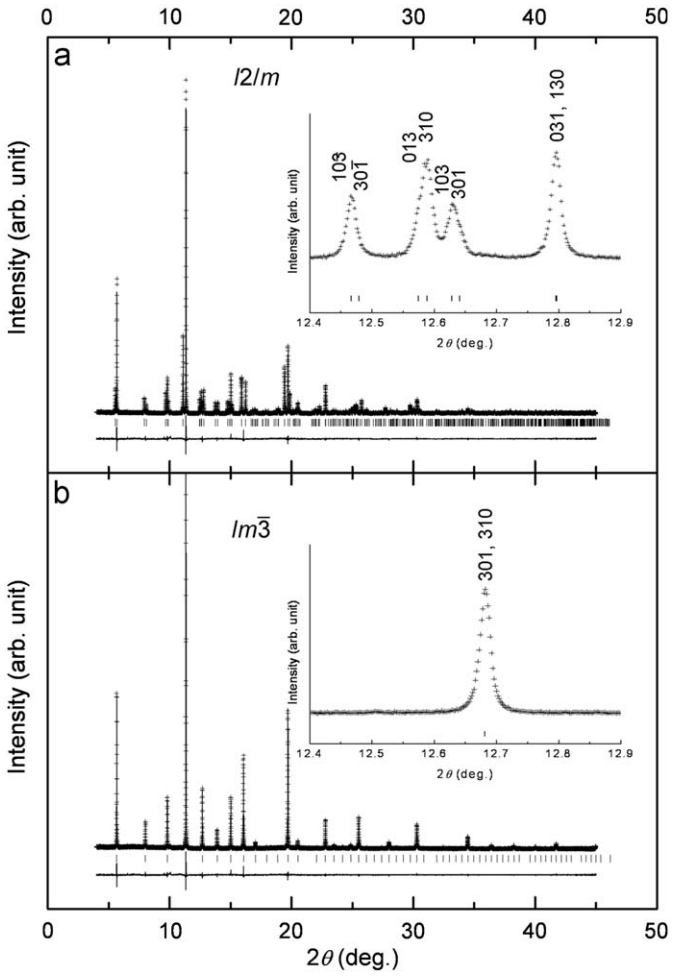

Fig. 2. Observed, calculated and difference intensity profiles from Rietveld refinement of high-resolution synchrotron X-ray diffraction data at room temperature for (a) monoclinic and (b) cubic $BiMn_7O_{12}$. The insets show reflections of importance for space group determination.

relevant Mn_4O_6 and Mn_5O_6 octahedra clearly suggest a (4+2)-type coordination (four short and two long bonds), *cf.* Table 2. This indicates a $3d_{x2-y2}$ type orbital ordering at the Mn *B*-site and so-called *d*-type orbital ordering as shown in Figs. 3(a) and (b).

Cubic phase: The HRSXRD pattern for the cubic phase is shown in Fig. 2(b). The indexing confirmed the single-phase nature of the sample satisfying the extinction rules for space group $Im\bar{3}$ (No 204): a=7.4471(1)Å; hkl: $h+k+l=2n$ [see inset to Fig. 1(b)] in agreement with previous reports [9,10]. The refined structural parameters are listed in Table 1. The initial refinements showed that the site occupancy and U_{iso} for Bi were strongly correlated. This refinement gave a large value for U_{iso}, i.e. $7.02(4)\times10^{-2}$ Å^2. Therefore, a split-atom description was adopted for the Bi-site by decreasing the point site symmetry from $m\bar{3}$ (Wyckoff position 2*a*) to 3 (Wyckoff position 16*f*). Then U_{iso} for Bi became quite reasonable, i.e. $2.3(14)\times10^{-2}$ Å^2. The Bi-displacements (involved in the symmetry lowering from $m\bar{3}$ to 3) are ~0.15 Å. The split-atom model yielded significantly improved values for reliability factors, R_{wp}=9.39%, R_p=7.26%, χ^2=1.53, and $R_F^2=10.3\%$. Upon further refinements the Bi-occupancy was reduced to 0.94(1), however, without influencing the need to use the split-atom model in order to properly model the Bi-position. Notably, the *R*-factors are not significantly improved upon refining the Bi-occupancy. In conclusion, the diffraction data sow no clear evidence for any reduced occupancy of the *A*′-site (see Table 1).

3.1. States of bismuth and manganese in the $BiMn_7O_{12}$ polymorphs

As described above, the initial structural refinements indicated tiny Bi-deficiencies corresponding to occupation numbers of 0.97(1) and 0.94(1) for the monoclinic and cubic polymorphs, respectively, in good accordance with the ICP analysis [14] that yields Bi:Mn ratios of 0.97(2):7.00(1) and 0.96(3):7.00(2). Considering the lack of conclusive evidence in the diffraction data (see above) and the uncertainty in the ICP data, we describe the polymorphs as close to stoichiometry but any smaller non-stoichiometry cannot be ruled out. The smaller unit-cell volume for cubic $BiMn_7O_{12}$ (413.0 Å^3 versus 416.8 Å^3 for monoclinic $BiMn_7O_{12}$) indicates a higher average oxidation state for Mn. Given an ideal O-sublattice, Bi non-stoichiometry might be envisaged from an electron neutrality point of view. A different explanation would be that some additional Mn is introduced to the Bi-site rather than vacancies; i.e. $[(Bi_{1-x}Mn_x)Mn_3]_{A\text{-site}}[Mn_4]_{B\text{-site}}O_{12}$, ($x\approx0$).

These two polymorphs are obtained *via* slightly different synthesis routes, and no information is currently available with respect to their relative thermal stabilities. In both polymorphs, the $Mn_{A''}O_{12}$ polyhedron (Figs. 1 and 3) has a basic square-planar building brick with the additional eight Mn–O bonds in a prismatic coordination at long separations (Tables 2 and 3).

Let us now compare the structural features of the monoclinic $BiMn_7O_{12}$ with those of the isostructural $LaMn_7O_{12}$. As seen from Table 1, its unit-cell volume of 416.8 Å^3 is very close to 416.9 Å^3 for $LaMn_7O_{12}$ [17]. This indicates that the ionic sizes of the Bi^{3+} and La^{3+} cations are very close and the Bi^{3+} ions should possess significant $6s^2$ lone-pair electron characters. Comparison of the bond distances in $LaMn_7O_{12}$ and $BiMn_7O_{12}$ (see Table 2) reveals an elongation of the distances between Bi and O3, and thus a crystal chemical impact of the involved hybridized state of the $6s^2$ lone-pair-electron dominated Bi^{3+} can be associated with these bond distances.

The formal oxidation states of the *A*″- and *B*-site Mn atoms can be evaluated from bond-valence-sum (BVS) calculations, by using the parameters [18] of $R_{ij}(Bi^{3+})$=2.09, $R_{ij}(La^{3+})$=2.172 and $R_{ij}(Mn^{3+})$=1.76, and bond distances of d_{ij} (see Tables 2 and 3) in the formula $\sum\exp[(R_{ij}-R_{ji})/0.37]$. The results indicate that all Mn atoms for the monoclinic and cubic polymorphs are trivalent (see Tables 2 and 3). Even though the BVS values for *A*″- and *B*-site Mn atoms in the monoclinic polymorph deviate slightly from the ideal value of three (see Table 2), the calculated average values for *A*″- and *B*-site Mn atoms of 2.94 and 3.19, respectively, are interestingly almost identical to those of the cubic phase (see Table 3). This is in good agreement with expectations, that is, the *A*″-site high-spin JT-active Mn^{3+} is stabilized for a highly distorted MnO_{12} coordination, and Mn^{3+} at the octahedral *B*-site is also JT-distorted in the monoclinic polymorphic. However, the BVS=2.22(5) for Bi in monoclinic $BiMn_7O_{12}$ (see Table 2) is significantly lower than anticipated, while BVS calculations correspond well to trivalent lanthanum in $LaMn_7O_{12}$. The bond distances in Table 2 suggest that the lowered BVS for Bi in monoclinic $BiMn_7O_{12}$ is due to elongation of the Bi–O3 bond. The deviation in BVS for Mn3 is due to over bonding between Mn3–O3, consistent with the observed under bonding between Bi–O3. As discussed above a large U_{iso} is obtained for O3 when all oxygen atoms are refined individually. Anisotropic displacement refinements give an unusually large value for U_{33} for O3. This may indicate a distribution of O3 displacements caused by the Bi lone-pair electrons. This observation is similar to those in $BiMnO_3$. Note that although the parameters used were not totally optimized, the BVS calculated values of ~3.2 for Bi in $BiMnO_3$ [average between 3.6 and 2.8 for the two sites], and ~3.2 in $BiCu_3Mn_4O_{12}$ are rather

Table 1
Unit cell dimensions and atomic coordinates for monoclinic and cubic $BiMn_7O_{12}$, derived from Rietveld refinement of high-resolution synchrotron X-ray diffraction data at room temperature.

Monoclinic						
Space group	I2/*m*					
Unit-cell parameters (Å)						
a	7.5191(1)					
B	7.3652(1)					
c	7.5284(1)					
β	91.225(1)					
Volume (Å^3)	416.82(5)					
Z	2					
Atom	Wyckoff position	*Occupancy*[a]	*x*	*y*	*z*	$100 \times U_{iso}$ (Å^2)[b]
Bi	2*a*	1	0	0	0	1.37(2)
Mn1	2*b*	1	0	1/2	0	2.40(4)
Mn2	2*c*	1	0	0	1/2	2.40(4)
Mn3	2*d*	1	0	1/2	1/2	2.40(4)
Mn4	4*e*	1	1/4	1/4	3/4	1.96(3)
Mn5	4*f*	1	1/4	1/4	1/4	1.96(3)
O1	4*i*	1	0.307(1)	0	0.165(1)	4.3(1)
O2	4*i*	1	0.319(1)	0	−0.173(1)	4.3(1)
O3	8*j*	1	−0.011(1)	0.183(1)	0.321(1)	4.3(1)
O4	8*j*	1	0.179(1)	0.311(1)	0.019(1)	4.3(1)
R_{wp} (%)	15.19					
R_p (%)	11.34					
χ^2	2.61					
Cubic						
Space group	$Im\bar{3}$					
Unit-cell parameters (Å)						
A	7.4471(1)					
Volume (Å^3)	413.02(1)					
Z	2					
Atom	Wyckoff position	*Occupancy*[a]	*x*	*y*	*z*	$100 \times U_{iso}$ (Å^2)
Bi	16*f*	1	0.0279(3)	0.0279(3)	0.0279(3)	2.3(1)
Mn1	6*b*	1	0	1/2	1/2	1.03(2)
Mn2	8*c*	1	1/4	1/4	1/4	0.79(2)
O	24*g*	1	0.3146(2)	0.1760(2)	0	0.99(5)
R_{wp} (%)	9.43					
R_p (%)	7.35					
χ^2	1.54					

[a] Occupancy of Bi, Mn, and O sites was fixed as 1 (see the detail on texts).
[b] Isotropic displacement parameters U_{iso} constrained at same values for respectively Mn *A*-site, Mn *B*-site and O.

Table 2
Selected inter-atomic distances (Å) and bond valence sum (BVS) for monoclinic AMn_7O_{12}, with *A*=Bi (present data) and *A*=La (Ref. [17]) included in [·] for comparison.

	Bi	Mn1	Mn2	Mn3	Mn4	Mn5
O1	2.60(10) × 2	2.875(9) × 2	3.45(10) × 2	1.92(10) × 2		1.999(3) × 2
	[2.612(4) × 2]	[2.847(4) × 2]	[3.427(4) × 2]	[1.954(4) × 2]		[1.989(17) × 2]
O2	2.76(10) × 2	2.83(11) × 2	3.40(10) × 2	1.85(10) × 2	1.997(4) × 2	
	[2.757(5) × 2]	[2.827(5) × 2]	[3.386(5) × 2]	[1.871(5) × 2]	[1.994(2) × 2]	
O3	2.778(7) × 4	3.364(7) × 4	1.905(7) × 4	2.688(8) × 4	1.923(8) × 2	2.110(8) × 2
	[2.707(3) × 4]	[3.368(3) × 4]	[1.904(3) × 4]	[2.764(3) × 4]	[1.912(3) × 2]	[2.121(3) × 2]
O4	2.662(7) × 4	1.936(7) × 4	2.791(7) × 4	3.336(7) × 4	2.158(7) × 2	1.859(7) × 2
	[2.636(3) × 4]	[1.935(3) × 4]	[2.820(3) × 4]	[3.340(3) × 4]	[2.150(3) × 2]	[1.869(3) × 2]
BVS[a]	2.22(5)	2.71(5)	2.96(6)	3.15(8)	3.02(5)	3.36(5)
	[3.10(3)]	[2.75(2)]	[2.97(2)]	[2.98(3)]	[3.08(2)]	[3.31(2)]
Polyhedra volume (Å^3)	49.7	44.0	44.6	40.6	11.0	10.4
	[48.3]	[44.2]	[44.3]	[42.6]	[10.9]	[10.5]
Δ[b]					23.5(05)	26.5(10)
					[23.9(06)]	[26.7(13)]

[a] Adopted bond-valence parameters of Bi^{3+}–O^{2-}, La^{3+}–O^{2-}, and Mn^{3+}–O^{2-} are 2.09, 2.172 and 1.76, respectively [18].
[b] The distortion parameter of Δ for octahedral coordinated MO_6 with and average *M*–O distance of $\langle M\text{–O}\rangle$, is defined as $\Delta=(1/6)\sum_{n=1-6}[(\text{Mn–O})-\langle \text{Mn–O}\rangle]/\langle \text{Mn–O}\rangle$.

close to the formal trivalent state [6,11]. For cubic $BiMn_7O_{12}$, BVS=2.60(2) was obtained for Bi (see Table 3).

Various AMn_7O_{12} compounds crystallize with different symmetries. There is a consistent variation as a function of ionic radius and/or oxidation state of the *A* species [10]; for $A'=Na^+$ the structure is cubic, for $A'=Ca^{2+}/Sr^{2+}/Cd^{2+}$ trigonal, and for $A'=La^{3+}$ monoclinic. For $A'Mn_7O_{12}$ there is a systematic trend in the tolerance factor with respect to the size of A' cation, i.e. the

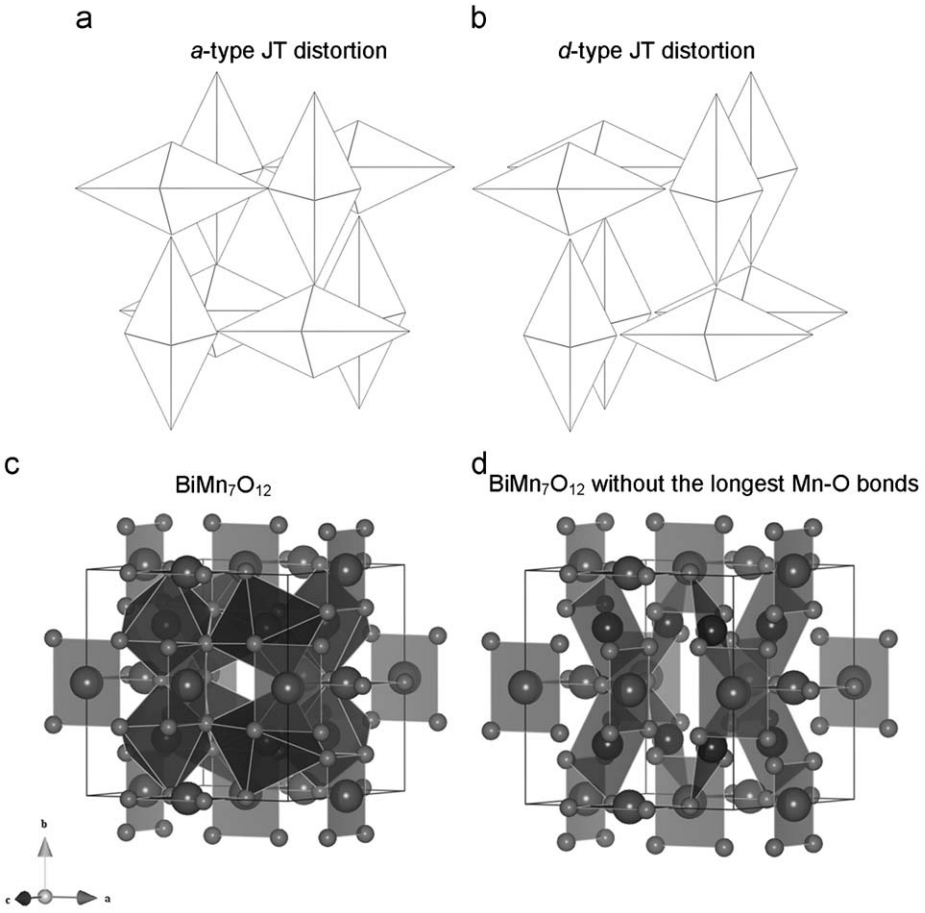

Fig. 3. Schematic drawing of crystal structure of (a) *a*-type, (b) *d*-type JT MnO_6 distortion, and (c) monoclinic $BiMn_7O_{12}$ [(d) same as (c) but without showing the longest Mn–O bonds of MnO_6 polyhedron].

Table 3
Selected interatomic distances (Å) for the split model description for cubic $BiMn_7O_{12}$.

	Bi	Mn1	Mn2
O	2.405(2) × 3	1.915(2) × 4	1.996(2) × 6
O	2.617(3) × 3	2.786(11) × 4	
O	2.770(3) × 3	3.351(15) × 4	
O	2.956(3) × 3		
BVS[a]	2.60(2)	2.93(16)	3.16(14)
Polyhedra volume (Å^3)	48.9	43.1	10.6

[a] Adopted bond-valence parameters of Bi^{3+}–O^{2-} and Mn^{3+}–O^{2-} are 2.09 and 1.76, respectively [18].

smallest (with Na^+) yields cubic symmetry and the largest (with La^{3+}) monoclinic symmetry. Simultaneously, the average size of *B*-site Mn increases in the said order (from Na^+ to La^{3+}) corresponding to the decrease in average Mn oxidation state. Another key issue for symmetry is the JT distortion of Mn^{3+} that occurs for trivalent *A*′-cations, i.e. only in $(La/Bi)Mn_7O_{12}$ with average Mn oxidation state +III. The cubic $BiMn_7O_{12}$ does not fall into this otherwise clear picture; here the *B*-site Mn oxidation state of +III is significantly lower than +3.5 as observed for cubic $NaMn_7O_{12}$. However, the *B*-site Mn atoms do not show sign of any JT distortion.

The bond distances for the cubic phase (calculated on the basis of the split-atom model; Bi in 16*f* (*x*,*x*,*x*); O in 24*g* (0,*y*,*z*)) are shorter than for the monoclinic polymorph, consistent with the contraction in the unit-cell volume. It appears likely that the rationale for an effective split-atom model in the Rietveld fit to the XRD data is the existence of the Bi^{3+} with $6s^2$ lone-pair effects. The lone-pair electrons are probably oriented randomly without any cooperative crystal-chemical effects. A major difference between the monoclinic and cubic $BiMn_7O_{12}$ polymorphs is that while all Mn^{3+} atoms for the monoclinic polymorph have a distorted arrangement as expected for JT active high-spin state of Mn(III), the *B*-site octahedral, Mn atoms have a regular arrangement in the cubic polymorph.

Two types of JT distortions relate to the orbital ordering schemes of simple perovskite, ABO_3. In these, the elongated axis of one octahedron connects to the short axis of a neighboring octahedron. For *d*-type JT distortions, the same arrangement of the elongation of the octahedra repeats in "layers" along one axis, whereas the elongation direction rotates 90° along the axis for *a*-type JT distortions (see Figs. 3(a) and (b)). The local structure surrounding a BO_6 octahedron depends hence on the type of JT distortion. It also depends on the BO_6 tilting scheme [19], e.g. the orthorhombic $GdFeO_3$-type scheme [20,21] that applies to $LaMnO_3$. The distortions may reflect orbital ordering in certain compounds, e.g. *a*-type JT distortion in $LaVO_3$ [22] and *d*-type in $LaMnO_3$ [23] and YVO_3 [24]. Any chemical pressure effects induced by substitution at the *A*-site influence also the distortion of the octahedral network, i.e. bond distances and angles. This notably affects the electronic properties such as orbital and spin orderings, and accordingly phase relations. *A*-site atoms with lone-pair electrons, e.g. $BiMnO_3$, may cause additional distortions, add complexity and functionality. For $BiMn_7O_{12}$ the situation

becomes even more complex than for the JT distorted perovskites due to magnetic Mn atoms in a highly distorted but basically square-planar environment at the A''-site (see Fig. 3). As previously discussed, monoclinic $BiMn_7O_{12}$ shows a d-type orbital ordering at the B-site with 4 short and 2 long Mn–O bonds, whereas quite regular MnO_6 octahedra are found for cubic $BiMn_7O_{12}$. The Mn^{3+} atoms at the A-site have basically a square-planar MnO_4 coordination forming a d_{x2-y2}-type orbital ordering. One would hence expect quite complicated orbital ordering schemes for the $Mn_{A''}$–O–Mn_B interactions which in turn depend on both the MnO_6-tilting and (JT-) distortions.

Experimentally it is seen that the monoclinic $BiMn_7O_{12}$ phase with $a^+b^+c^+$ type tilting and d-type JT distortion is tightly correlated with orbital ordering in the MnO_6 octahedral network. This is analogous to that of isomorphic $LaMn_7O_{12}$ for which the JT distortion [17] is relaxed through a first order structural phase transition at $\sim$380 °C. Figs. 3 (c) and (d) show the corner-sharing of Mn_BO_6 and MnO_4 polyhedrons. These figures show coordination polyhedra drawn, respectively, with and without the longest Mn_B–O bonds of the 4+2 distorted octahedra. Due to the d-type JT the connectivity of the $Mn_{B\text{-site}}O_6$ and $Mn_{A''}O_4$ polyhedra becomes very complex. The unusually large values of U_{iso} for O3 and O4 could possibly be explained on this basis. Interestingly, O3 and O4 are involved in the longest bonds of the 4+2 MnO_6 octahedra. Different kinds of charge distribution between $Mn_{A''}$–O–Mn_B together with the d-type JT distortion scheme may explain the anisotropic behavior of U_{ij} for O3 and O4. The key to understand the monoclinic $BiMn_7O_{12}$ will also include the coordination of $Mn_{A''}O_4$ and/or extra Mn–O bonds *via* $Mn_{A''}$–O–Mn_B, not only Mn_BO_6 octahedra as in the case of simple perovskites. One expects different electronic properties (magnetic structure inclusive) for cubic and monoclinic $BiMn_7O_{12}$, due to e.g. complex super-exchange interactions for $Mn_{A''}$–O–Mn_B at low temperatures. These are likely influenced by orbital/charge ordering in the MnO_4 planes of the Mn_BO_6 and $Mn_{A''}O_{12}$ coordinations due to the unique d-type JT distortions, and complex Mn–O connectivity. This contrary to the situation in Cu-based cubic ($Im\bar{3}$) $ACu_3B_4O_{12}$ phases with (A, B)=(Bi, Mn) [11], (Ca, Mn) [24–28], (Tb, Mn) [29], (La, Fe) [30], and (Ca, Ti/Ge/Sn) [31] which are in a relaxed state (i.e. no elongation of the octahedra). Due to the presence of unique $Mn_{A''}O_{12}$ coordination in the present structure, an extra super-exchange path may be present in $Mn_{A''}$–O–Mn_B besides the conventional Mn_B–O–Mn_B.

4. Conclusions

The present analysis of HRSXRD data indicate that $6s^2$ lone-pair electrons of Bi^{3+} have a certain crystal chemical effect in both the monoclinic and cubic $BiMn_7O_{12}$ polymorphs. No strong cooperative crystal-chemical effects arise from the lone-pair electrons, however, average chemical bonds seemed to be elongated as revealed through comparison of crystal data for $BiMn_7O_{12}$ and $LaMn_7O_{12}$. Unusually large (and anisotropic) displacement parameters for some of the oxygen atoms in the monoclinic phase may indicate competition between non-equivalent Mn–O bonds for the corner-sharing d-type JT Mn_BO_6 and the square-planar $Mn_{A''}O_4$ polyhedra. No indications were found for off-centering of Bi in the monoclinic phase, whereas a split model was required for the cubic polymorph. The MnO_4 unit is likely to induce additional interactions via the $Mn_{A''}$–O–Mn_B bonds. Careful investigations by means of powder neutron diffraction and transmission electron microscopy are required to confirm the present findings, in particular for clarifying whether slight departures from stoichiometric composition could exist for one of the polymorphs.

Acknowledgments

This work was supported by the Research Council of Norway, Grant No. 158518/431 (NANOMAT), and also by Tekes (No. 1726/31/07) and Academy of Finland (Nos. 114517, 116254 and 126528). We highly acknowledge the assistance of the research team at the Swiss–Norwegian Beam Lines, ESRF.

Appendix A. Supplementary data

Supplementary data associated with this article can be found in the online version at doi:10.1016/j.jssc.2009.10.013.

References

[1] T. Yokosawa, A.A. Belik, T. Asaka, K. Kimoto, E. Takayama-Muromachi, Y. Matsui, Phys. Rev. B 77 (2008) 02411.
[2] F. Sugawara, S. Iiida, Y. Syono, S. Akimoto, J. Phys. Soc. Jpn. 25 (1968) 2553.
[3] A. Moreira dos Sants, A.K. Cheetham, T. Atou, Y. Syono, Y. Yamaguchi, K. Ohoyama, H. Chiba, C.N.R. Rao, Phys. Rev. B 66 (2002) 064425.
[4] T. Kimura, S. Kawamoto, I. Yamada, M. Azuma, M. Takano, Y. Tokura, Phys. Rev. B 67 (2003) 180401.
[5] R. Seshadri, N.A. Hill, Chem. Mater. 13 (2001) 2892.
[6] T. Atou, H. Chiba, K. Ohoyama, Y. Yamaguchi, Y. Syono, J. Solid State Chem. 145 (1999) 639.
[7] E.O. Wollan, Phys. Rev. 100 (1955) 545.
[8] R.D. Shannon, Acta Crystallogr. Sect. A 32 (1976) 751.
[9] M. Marezio, P.D. Dernier, J. Chenavas, J.C. Joubert, J. Solid State Chem. 6 (1973) 16.
[10] B. Bochu, J. Chenavas, J.C. Joubert, M. Marezio, J. Solid State Chem. 11 (1974) 88.
[11] K. Takata, I. Yamada, M. Azuma, M. Takano, Y. Shimakawa, Phys. Rev. B 76 (2007) 024429.
[12] N. Imamura, M. Karppinen, T. Motohashi, D. Fu, M. Itoh, H. Yamauchi, J. Am. Chem. Soc. 130 (2008) 45.
[13] F. Mezzadri, G. Calestani, M. Calicchio, E. Gilioli, F. Bolzoni, R. Cabassi, M. Maresio, A. Migliori, Phys. Rev. B 79 (2009) 100106.
[14] N. Imamura, M. Karppinen, H. Yamauchi, Chem. Mater. 21 (2009) 2179.
[15] H.M. Rietveld, J. Appl. Crystallogr. 2 (1969) 65.
[16] A.C. Larson, R.B. Von Dreele, Los Alamos National Laboratory Report LAUR, 86, 2000, p. 748.
[17] H. Okamoto, M. Karppinen, H. Yamauchi, H. Fjellvåg, Solid State Sci. 11 (2009) 1211.
[18] N.E. Brese, M. K'Keeffe, Acta Crystallogr. Sect. B 47 (1991) 192.
[19] A.M. Glazer, Acta Crystallogr. Sect. A 31 (1975) 756.
[20] J.B. Goodenough, Magnetism and the Chemical Bond, Wiley, New York, 1963.
[21] J.B. Goodenough, J. B. Phys. Rev. 100 (1955) 564.
[22] P. Bordet, C. Chaillout, M. Marezio, Q. Huang, A. Santoro, S.W. Cheong, H. Takagi, C.S. Oglesby, B. Batlogg, J. Solid State Chem. 106 (1993) 253.
[23] H. Kawano, H. Yoshizawa, Y. Ueda, J. Phys. Soc. Jpn. 63 (1994) 2857.
[24] J. Chenavas, J.C. Joubert, M. Marezio, B. Bochu, J. Solid State Chem. 14 (1975) 25.
[25] Z. Zeng, M. Greenblatt, Phys. Rev. Lett. 82 (1999) 3164.
[26] W. Slawinski, R. Przenioslo, I. Sosnowska, M. Bieringer, I. Margiolaki, A.N. Fitch, E. Suard, J. Solid State Chem. 179 (2006) 2443.
[27] R. Przenioslo, M. Regulski, I. Sosnowska, R. Schneider, J. Phys. Cond. Mater. 14 (2002) 1061.
[28] J. Sanchez-Benitez, J.A. Alonso, M.J. Martinez-Lope, M.T. Casais, J.L. Martinez, A. de Andres, M.T. Fernandez-Diaz, Chem. Mater. 15 (2003) 2193.
[29] J. Sanchez-Bentez, J.A. Alonso, A. de Andres, M.J. Martnz-Lope, J.L. Martinez, A. Munoz, Chem. Mater. 17 (2005) 5070.
[30] Y.W. Long, N. Hayashi, T. Saito, M. Azuma, S. Muranaka, Y. Shimakawa, Nature 458 (2009) 60.
[31] M. Mizumaki, T. Saito, H. Shiraki, Y. Shimakawa, Inorg. Chem. 48 (2009) 3499.